The effect of annealing time on the structural and optical properties of $ZnAl_2O_4$:0.01% Cr^{3+} nanophosphor prepared via sol-gel method

S.V. Motloung[*1], S.J. Motloung[2], H.C. Swart[3], T. T. Hlatshwayo[4]

[1]Department of Physics, Sefako Makgatho Health Science University, P. O. Box 94, Medunsa, 0204, South Africa

[2]Department of Physics, University of the Free State (Qwaqwa Campus), Private Bag X13, Phuthaditjhaba, 9866, South Africa

[3]Department of Physics, University of the Free State, P.O. Box 339, Bloemfontein, 9300, South Africa

[4]Department of Physics, University of Pretoria, Pretoria, 0002, South Africa

Corresponding author:

Tel:+27 72 920 4758. E-mail: cchataa@gmail.com (Setumo Victor Motloung)

Abstract

Zinc aluminate ($ZnAl_2O_4$) host and 0.01% Cr^{3+} doped were successfully prepared using the sol-gel method. The annealing time (AT) was varied in the range of 0.5 - 19 h. The X-ray diffraction results showed that the AT does not affect the crystal structure of the prepared powders. Scanning electron microscopy (SEM) results showed that the morphology of the prepared nanophosphors was influenced by the AT. Energy dispersive x-ray spectroscopy (EDS) confirmed the homogeneous distribution of the constituent elements. Transmission Electron microscopy (TEM) suggested that the average crystallites sizes of the $ZnAl_2O_4$ to be ~ 20 nm. Ultraviolet- visible (UV-Vis) spectroscopy results revealed that the bandgap (E_g) of the prepared nanophosphor can be tuned by varying the AT. The emission peak at 390 nm is attributed to the intrinsic defects within the host material bandgap. The emission peak at 572 nm is attributed to both contribution from the host and Cr^{3+} ($^4T_1 \rightarrow {}^4A_2$) transition. The maximum PL intensity was observed from the samples annealed for 3 h. The International Commission on Illumination (CIE) chromaticity diagram showed a slight shift on the blue emission with an increase in AT.

Keywords: Luminescence; $ZnAl_2O_4$:0.01% Cr^{3+}; Phosphor; Sol-gel; Annealing time

1. Introduction

Zinc aluminate ($ZnAl_2O_4$) is a spinel type oxide and a wide-band gap semiconductor with an optical band gap of 3.8 eV [1,2]. $ZnAl_2O_4$ is a suitable material for a wide range of applications which includes its use in photoelectric devises, catalysts, electroluminescence displays, optical coating and highly efficient phosphor materials [3-5]. $ZnAl_2O_4$ is one of the spinels that is known as a suitable host lattice for dopants or foreign atoms [6-8]. The optical properties of the resulting phosphor materials is governed by many factors such as the activator type, concentration, distribution, host material crystal structure and crystallite sizes [8]. Kumar et al. [9] prepared the blue emitting $ZnAl_2O_4$:Ce^{3+} nanophosphor via citrate sol-gel

method. The PL emission spectrum of Ce^{3+} doped $ZnAl_2O_4$ nanophosphor with excitation of 300 nm exhibited an intense asymmetric broad emission band ranging from 320-400 nm with the intense peak at 360 nm in the blue-violet region. The band around 350 nm was attributed to the 5d ($^2D_{3/2}$) $\rightarrow^4$f ($^2F_{5/2}$, $^2F_{7/2}$) transition due to Ce^{3+} ions. It was suggested that the single exponential decay time indicates that the Ce^{3+} ions are occupying a single site in the $ZnAl_2O_4$ host. $ZnAl_2O_4$:x% Eu^{3+} nanophosphor have also been developed by Fernandez-Osorio et al. [10] and the results suggested that the transition at 586 and 616 nm respectively originates from a magnetic dipole ($^5D_0 \rightarrow ^7F_1$) and electric dipole ($^5D_0 \rightarrow ^7F_2$) transitions in Eu^{3+}. Brik et al. [11] studied the luminescence of Cr^{3+} ions in $ZnAl_2O_4$ and $MgAl_2O_4$ spinels prepared by self-propagating high temperature synthesis. The correlation between experimental spectroscopic studies and crystal field calculations were investigated in details. The results showed that both compounds emits at around 685 nm due to the $^2E_g \rightarrow ^4A_{2g}$ spin-forbidden transition of Cr^{3+} ions located at the sites with D_{3d} local symmetry. Our group [8] previously prepared the $ZnAl_2O_4$:x% Cr^{3+} nanophosphor via the sol-gel method and the emission spectra revealed that all the powder samples exhibited a violet emission. The 396 nm emission peak was ascribed to the intrinsic intraband gap defects. As the Cr^{3+} was increased, the emission peak slightly shifted to 401 nm, which suggested that the emission was originating from both the host as well as the Cr^{3+} ions. The emission from Cr^{3+} ions was attributed to arise from the $^4T_1 \rightarrow ^4A_2$ transition. The emission peak at 566 nm was assigned to be from the 2nd order emission or $^4T_2 \rightarrow ^4A_2$ transition from Cr^{3+}. The emission peak at 692 nm was assigned to the R-lines of $^2E \rightarrow ^4A_2$ transition in Cr^{3+} ions. The optimum PL intensity was found for the sample doped at 0.01% Cr^{3+} ion, which serves as the main reason why 0.01% Cr^{3+} was considered in this study. The effects of annealing temperature on the structural, optical and thermoluminescent (TL) properties of $ZnAl_2O_4$:Cr^{3+} phosphor have been reported by Rani et al. [12]. The intense luminescence lines in PL spectra of $ZnAl_2O_4$: Cr^{3+} spinel revealed that the Cr^{3+} ions are located in the sites with octahedral symmetry. Different methods such as solid state reaction [13], hydrothermal synthesis [14], combustion process [15], co-precipitation [16], sol-gel [17] and microwave [18] have been proposed in literature for the fabrication of $ZnAl_2O_4$. As an alternative, sol-gel route was employed in this study due to its simplicity and advantages of being able to produce nanopowders at a very low temperature [19].

To the best of our knowledge, the effect of AT on the luminescence and structural properties of $ZnAl_2O_4$:0.01% Cr^{3+} have not been reported in the literature. This research focused on the effect of AT on $ZnAl_2O_4$:0.01% Cr^{3+} with the aim of fabricating or developing new nanophosphor materials for the applications such as in light emitting diodes (LED's).

2. Experimental

Undoped ($ZnAl_2O_4$) and $ZnAl_2O_4$:0.01% Cr^{3+} nano powders were synthesized via sol-gel technique using citric acid (CA) as a chelating agent. Undoped sample was prepared by dissolving $Zn(NO_3)_2 \cdot 6H_2O$ (98%), $Al(NO_3)_3 \cdot 9H_2O$ (98%) and CA, $C_8H_8O_7 \cdot H_2O$ (99%) in deionized water while the 0.01% Cr^{3+} doped samples were prepared by adding $Cr(H_2O)(NO_3) \cdot 3H_2O$ (98%) to the solutions of the undoped. The molar ratio of Zn:Al was 1:2, and molar ratio of Zn: CA was 1:3. All the solutions were heated below 80 ^{o}C with constant stirring on a magnetic stirrer until the gels were formed. The gels were then transferred to a muffle furnace which was set at 800 °C for various AT (0.5 - 19 h). The resulting powder samples were then cooled to room temperature and crushed with a pestle and mortar. The samples were ready for the characterization with different techniques. The powder X-ray diffraction (XRD) (Bruker AXA

Discover diffractometer) with CuKα (1.5418 nm) radiation was used to investigate the crystal structure of the samples. The surface morphology and elemental composition of the nanophosphor powder were investigated using a Shimazu Super scan ZU SSX-550 electron microscope (SEM) coupled with an electron diffraction spectroscopy (EDS). High-Resolution Transmission Electron microscopy (HR-TEM) was performed with a JOEL JEM 2100 containing a LaB6 filament to study the morphology. UV-Vis diffuse reflection spectroscopy was used to study the absorption characteristics of the prepared samples. PL spectra were recorded at room temperature using a Hitachi F-7000 fluorescence spectrophotometer.

3. Results

3.1 X-Ray diffraction

The XRD patterns of the 0.01% Cr^{3+} doped and un-doped $ZnAl_2O_4$ annealed at 800°C for various AT (0.5 - 19h) are presented in Fig. 1. The patterns are consistent with the standard data for cubic $ZnAl_2O_4$ spinel phase (JCDPS: 82-1043). The same phases without impurities were observed for all samples. Fig. 1. (b) illustrates the analysis of the most intense diffraction peak (311). Generally and as the AT increases, the peak shift to the higher diffraction angle is observed and this can be attributed to the decrease in lattice parameter. This may be due to the crystal ordering as the AT increased. The alteration on the (311) diffraction peak intensity is related to the variation on the crystalline quality [8]. Hence, it is clear that the AT influences the crystallinity of the prepared nanophosphors. The crystallite sizes were estimated using the well-known Scherrer's formula [20] given in equation (1):

$$D = \frac{0.9\lambda}{\beta \cos \theta} \tag{1}$$

where D is the crystallite size (nm), λ stands for the radiation wavelength (0.15406 nm), β is the full width at half maximum (in radians), and θ is the angle of diffraction (in degrees). The crystallite size values, as estimated from the (311) diffraction peak, are presented in Table I. This results showed that AT affected the crystallite size.
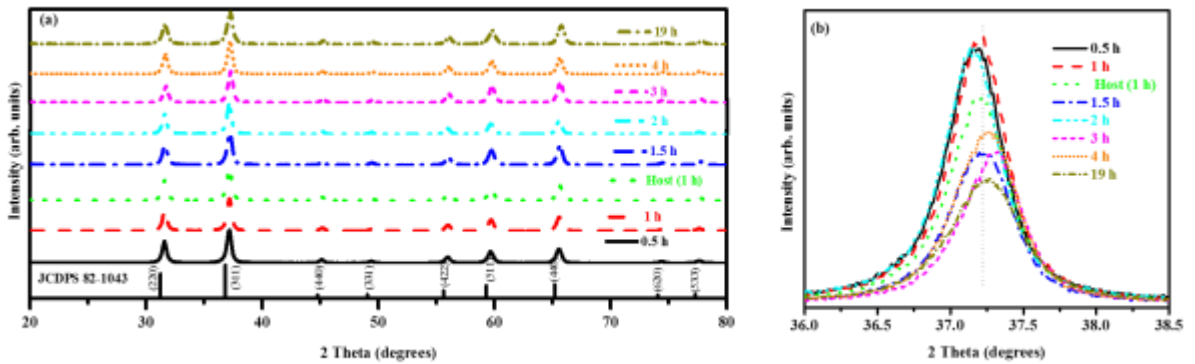

Fig. 1. (a) XRD patterns of the un-doped and $ZnAl_2O_4$:0.01% Cr^{3+} (0.5 - 19 h) and (b) analysis of (311) diffraction peak.

Table I. Summary of the samples identification, crystallites size and decay times.

AT (h)	Crystallites size (nm)	Decay times (ms)		CIE coordinates
		τ_1	τ_2	(x;y)
0.5	21	516.6 ± 0.4	1534.4 ± 297.9	(0.182;0.162)
1*	22	516.9 ± 0.4	1455.7 ± 297.0	(0.177;0.151)
1	19	518.3 ± 0.6	1200.3 ± 227.2	(0.177;0.151)
1.5	20	518.9 ± 0.7	1173.7 ± 216.1	(0.172;0.140)
2	21	519.2 ± 0.7	1198.0 ± 209.7	(0.172;0.140)
3	20	523.8 ± 1.5	921.4 ± 103.9	(0.168;0.124)
4	19	522.4 ± 1.3	931.9 ± 112.8	(0.169;0.122)
19	17	523.5 ± 1.0	993.5 ± 97.5	(0.176;0.150)

*Un-doped sample

3.2 EDS and EDS mapping

The EDS spectra of the un-doped $ZnAl_2O_4$ and $ZnAl_2O_4$:0.01% Cr^{3+} samples annealed at the AT = 1 h are illustrated in Fig. 2. In Fig. 2 (a), all of the as-designed elements Zn, Al and O are evidently noticed for the un-doped or host sample. As anticipated, Fig. 2 (b) presents the $ZnAl_2O_4$:0.01% Cr^{3+}, which clearly shows the presence of the Cr. The additional peak of carbon (C) present in all samples shown in Fig. 2 is due to fact that samples were mounted on the carbon tape during EDS measurements. The EDS did not detect any other impurities in the samples, which agrees well with the XRD results shown in Fig. 1. Furthermore, the EDS mapping was used to confirm the composition and distribution of the constituent elements of the powder samples. Fig. 3 (a) and (b) respectively shows the EDS maps for the un-doped and $ZnAl_2O_4$:0.01 % Cr^{3+} samples. In both maps, it can be seen that the all compositional elements are homogenously distributed on the surface.
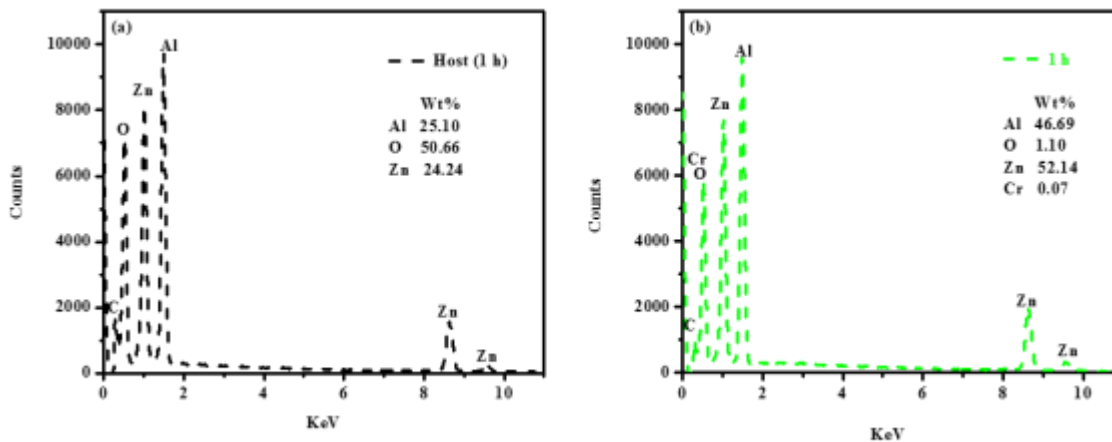
Fig. 2. The raw EDS spectra for the (a) host and $ZnAl_2O_4$:0.01 % Cr^{3+} samples at AT = 1 h.

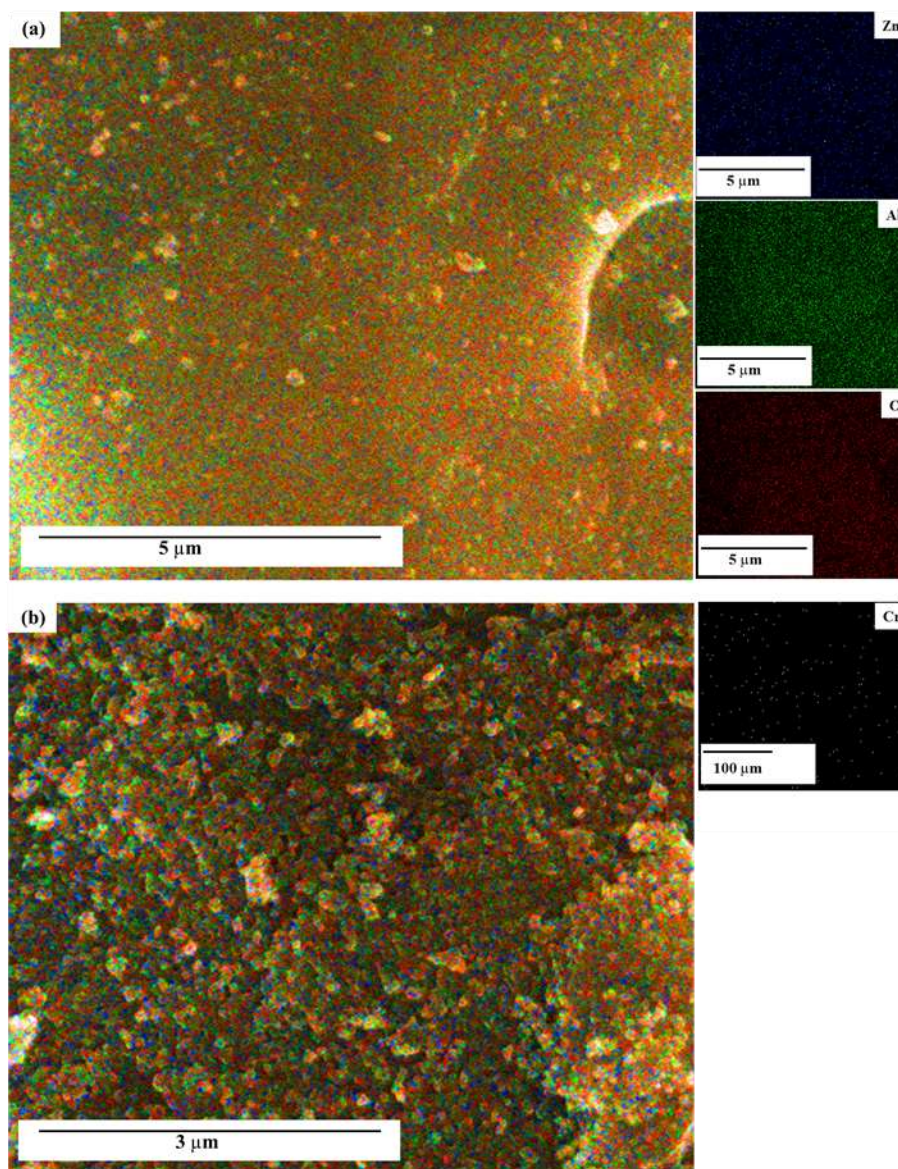**Fig. 3.** EDS mapping images for the (a) un-doped and (b) ZnAl$_2$O$_4$:0.01% Cr^{3+} (red (O), green (Al), blue (Zn) and white (Cr)).

3.3 SEM and TEM

Fig. 4 shows the SEM micrographs for un-doped and ZnAl$_2$O$_4$:0.01% Cr^{3+} powders annealed at various AT. The un-doped ZnAl$_2$O$_4$ (host) at AT = 1 h consist of irregular particle sizes distribution all over the surface as shown in Fig. 4 (a). For the ZnAl$_2$O$_4$: 0.01% Cr^{3+} at AT = 1 h, the degree of the irregular crystal particles agglomeration seems to be more pronounced. At the AT = 3 h, the crystallites particles are agglomerating more or parked to form bigger crystalline particles compared to AT = 1 h. For the higher AT = 19 h, the crystallites particles have formed a bigger smooth brittle-like morphologies. Thus, it is clear that doping and AT influences the morphology of the prepared nanophosphors.
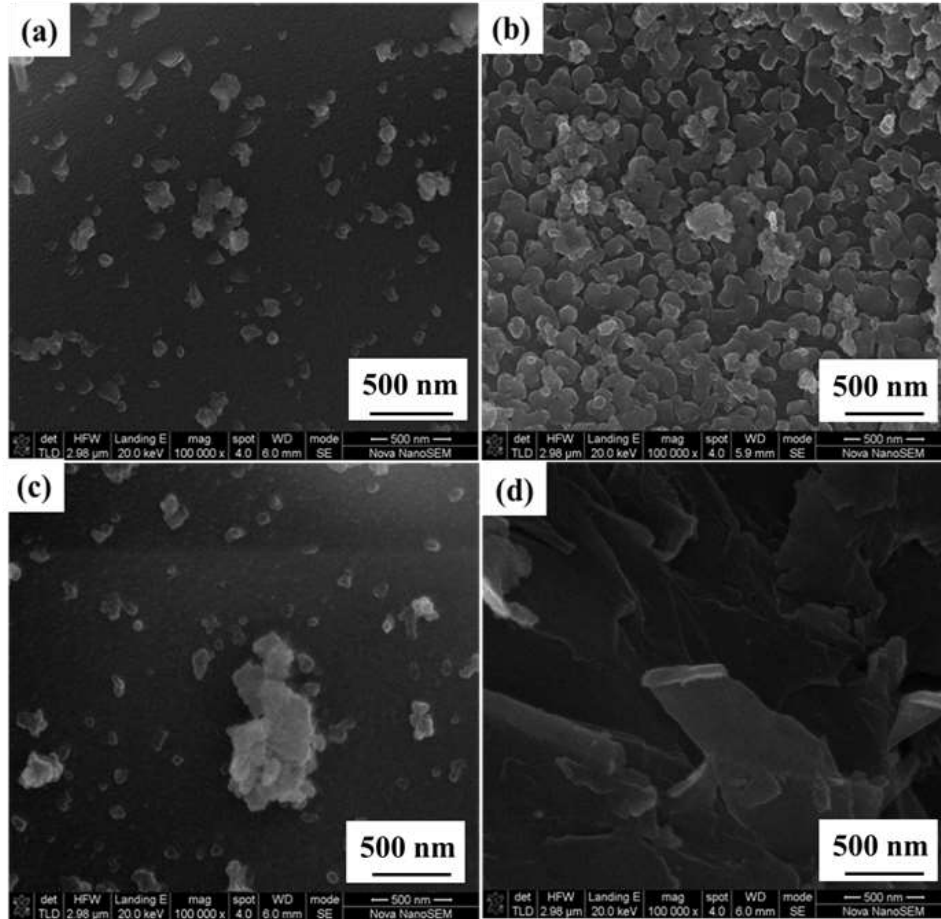
Fig. 4. SEM photographs of the (a) un-doped (AT = 1 h), (b) $ZnAl_2O_4$:0.01% Cr^{3+} at AT (b) 1 h, (c) 3 h and (d) 19 h.
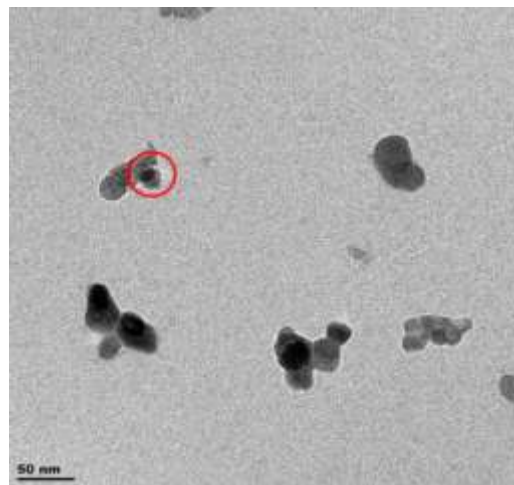

Fig. 5. The TEM image for the host ($ZnAl_2O_4$) at AT = 1 h.

TEM image of the host sample (AT = 1h) is shown in Fig. 5. It is clearly observed that the powder sample consists of the nanocrystals. These results suggest that the average crystallites sizes were approximately

around 20 nm, which is very close to the estimated by the XRD results. In addition, the nanocrystals structure (indicated by the red circles) is observed to be cubic-like, which agrees very well with the cubic structure of $ZnAl_2O_4$ (JCDPS: 82-143) described on the the XRD results. Therefore, the TEM and XRD results are in agreement with the XRD findings.

3.4 UV- Vis

The UV-Vis diffuse reflection spectroscopy results are shown in Fig. 6 (a). There are three absorption bands located around 231, 310 and 370 nm. Both absorption bands at 231 and 370 nm are attributed to arise from the band-to-band transition and defects absorption within the host material, respectively [8]. The sharp band at 310 nm appears as a results of the lamp changing to the other lamp on the UV-Vis system.

In order to transform the reflectance to the values proportional to absorbance, the Kubelka-Munk (K-M) function $K = (1- R^2)/(2R)$ was used (where K is K-M absorption coefficient and R is reflectance). The E_g of the prepared samples can be estimated from the plots of $(K \times h\nu)^n$ ($n = 2$ for a wide bandgap semiconductor such as $ZnAl_2O_4$) against $h\nu$ (where h is the Planck constant and ν is the frequency). The linear portions of the plots are extrapolated to the $h\nu$ axis as shown in Fig. 6 (b) to estimate or obtain the values of the E_g [21,22]. The results indicate that the E_g of the prepared samples depend on the AT and the E_g can be tuned between 2.80 - 3.06 eV by varying AT in a range (0.5-19 h).
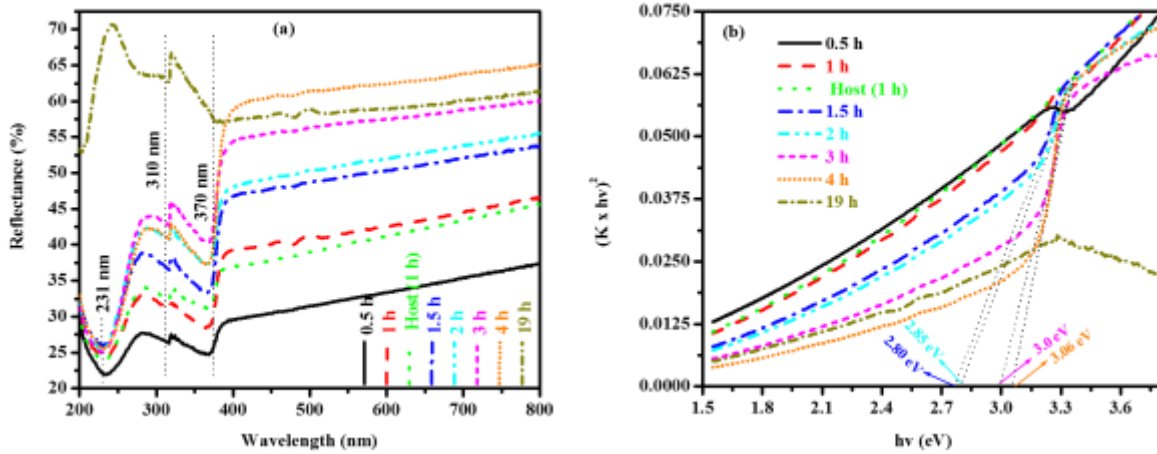

Fig. 6. (a) The diffuse reflectance spectra of the un-doped and $ZnAl_2O_4$:0.01% Cr^{3+} annealed at various periods (0.5 - 19 h) samples, (b) estimate of the direct optical bandgap of the samples in (a) using Kubelka-Munk function [22].

3.5 Photoluminescence

The PL excitation and emission spectra for the 0.01% Cr^{3+} doped and un-doped $ZnAl_2O_4$ annealed at 800 ^{o}C at various AT is presented on Fig. 7 (a). When monitoring an emission peak at 390 nm, there were three excitation peaks observed at 231 nm, 282 nm, and 330 nm. As discussed on the UV-Vis results, the 231 nm excitation peak is certainly attributed to the band-to-band transition from the host material. This results suggests that at the high AT the band-gab energy increased since the 231 nm peak is only observed at AT = 19 h. The excitation peaks at 282 nm and 330 nm are both attributed to the $ZnAl_2O_4$ bandgap defects levels (DL) (see Fig. (i) and (ii)), respectively [7]. When exciting the samples at 282 nm, there are two emission peaks located around 390 and 572 nm. The emission peak at 390 nm is ascribed to the

intrinsic bandgap defects such as oxygen vacancies on the host material (see Fig. 8.) [8]. The 572 nm emission peak is suggested to be from the Cr^{3+} ions and host defects [8]. This peak is more intense at AT = 19 h as shown on the normalized emission spectra in Fig. 7 (b). This results suggest that at the higher AT (19 h) the traps located at 2.17 eV (572 nm) are starting absorbing more excited electron. However, the reason for this behavior needs further investigations. The 572 nm emission specifically from the Cr^{3+} is assigned to the $^4T_2 \rightarrow {}^4A_2$ transmission [8]. Comparing the host and 1 h (doped) samples, and as anticipated from [8], it can be seen that the emission intensity for the host material is lower than that of the doped sample and this may be due to insufficient luminescence centers on the un-doped sample. When the AT increases, the emission intensity also increases and reaches its maximum at 3 h as shown in Fig. 7 (c). This suggests that effects of the AT on the prepared material is behaving in the same or typical way as the effects of the dopant concertation since both the luminescence enhancement and quenching are both observed. The emission channels is summarized in Fig. 8 (where NRR refers to the non-radiative recombination). It is therefore concluded that the AT affects the luminescence properties of the $ZnAl_2O_4$:0.01% Cr^{3+} nanophosphor. Fig. 9 presents the emission spectra of the AT = 3 h at various excitations. It is clear from Fig. 9 (a) and the deconvolution (green dotted line) in Fig. 9 (b) that the optimum excitation wavelength is obtained at 282 nm and this serves as an appropriate or additional reason as to why all the samples were where excited at 282 nm.
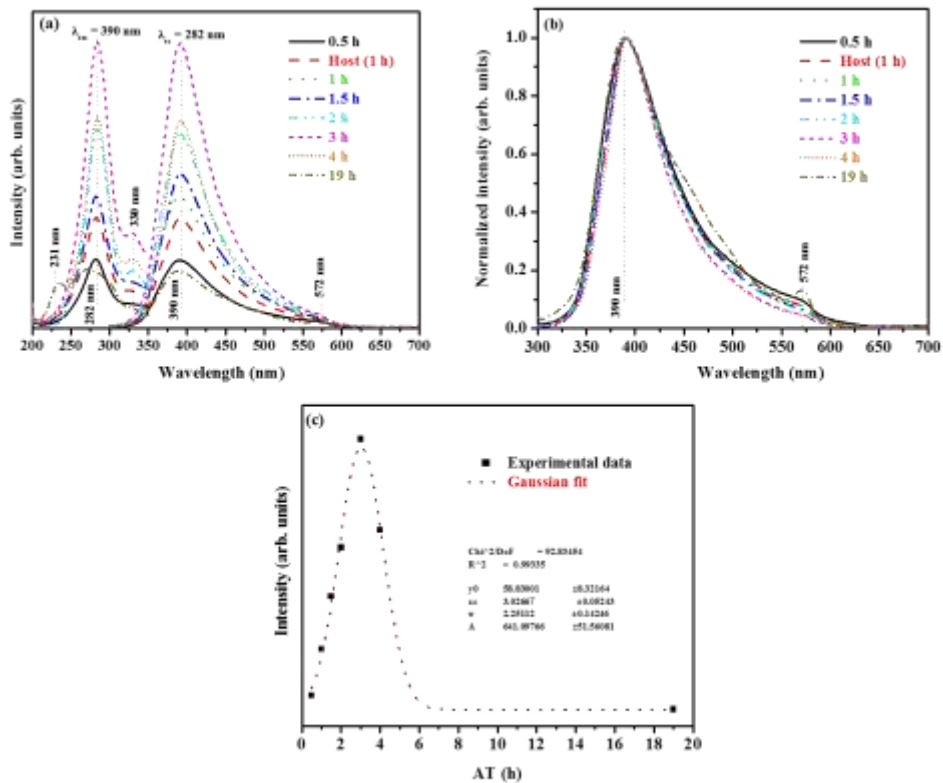

Fig. 7 (a) The excitation and emission spectra of $ZnAl_2O_4$:0.01% Cr^{3+} nano-phosphor annealed at different times, (b) normalized emission intensity as a function of wavelength and (c) intensity as a function of AT.
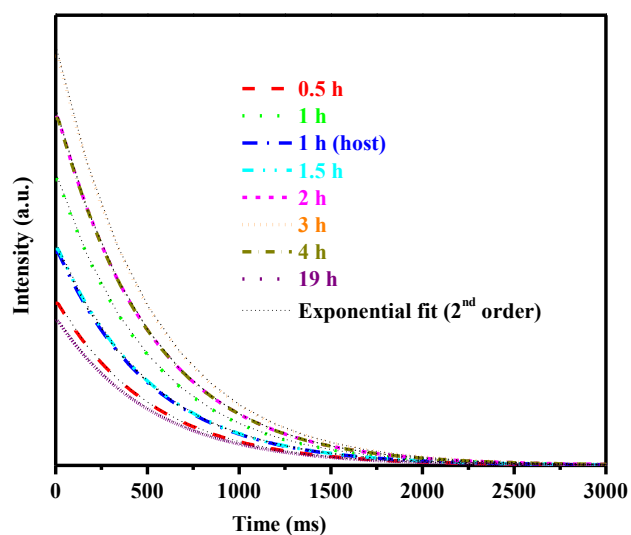
The decay curve of the un-doped and 0.01% Cr^{3+} doped $ZnAl_2O_4$ at various AT is presented in Fig. 10. When all the decay curves are compared, it is clearly observed that the decay characteristics of these phosphors are similar, which suggests that all the samples have the same afterglow decay mechanism as seen in report [21]. The calculated decay times are presented in Table I. The second order exponential decay given in Eq. (2) was used for fitting all the decay curves.

$$I(t) = I_0 + A_1 e^{\left(-t/\tau_1\right)} + A_2 e^{\left(-t/\tau_2\right)}$$

$\cdots$

(2)

where I represents the phosphorescent intensity, I_0 is the luminescence intensity initially, A_1, A_2 are constants, t is the time of measurement, and τ_1, τ_2 are the decay time values [23]. The results are consistent with the measurements of the PL emissions in Fig.7 (a), in which the sample annealed at 3 h was observed to have the highest emission intensity.

Fig. 8. The phosphor emission pathways mechanism for $ZnAl_2O_4$:0.01% Cr^{3+} ion.

Fig. 9. Experimental data (for AT = 3 h), (a) the emission spectra of $ZnAl_2O_4$:0.01% Cr^{3+} at different excitations and (b) the intensity as a function of excitation wavelength.

9

Fig. 10. The decay curve of un-doped and $ZnAl_2O_4$:0.01% Cr^{3+}.

The CIE chromaticity diagram for the prepared samples is shown in Fig. 11. The CIE Coordinates calculator software [24] was employed to determine the (x;y) co-ordinates and the values are presented in Table I. The CIE confirmed that the blue emission of the $ZnAl_2O_4$:0.01% Cr^{3+} nanophosphor can be tuned slightly by varying the AT.
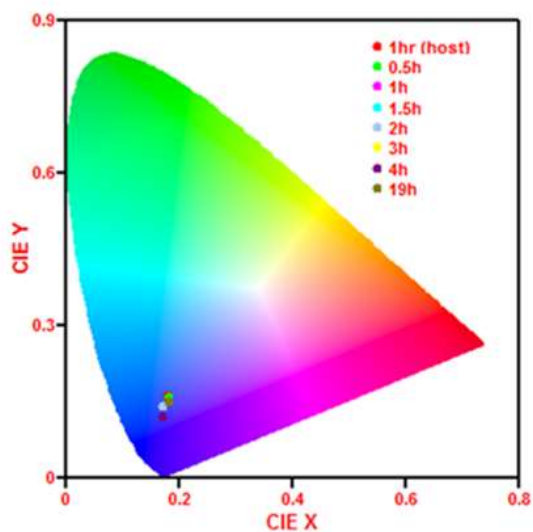

Fig. 11. CIE chromaticity diagram for $ZnAl_2O_4$ (host) and $ZnAl_2O_4$:0.01% Cr^{3+} nano-powders at various AT (0.5-19h).

10

4. Conclusion

$ZnAl_2O_4$ and $ZnAl_2O_4$:0.01 %Cr^{3+} nanophosphors were successfully prepared via the sol-gel method with citric acid as a chelating agent. The XRD and TEM analysis confirmed that the prepared nanophosphors consisted of the cubic structures. The phosphor surface morphology, bandgap and crystallite sizes were influenced by varying the AT. The PL results confirmed that the emission resulting from the prepared phosphor materials originate from both the host material and Cr^{3+} transition. The optimum emission intensity was observed at AT is 3 h. The CIE coordinates revealed that the blue emission color of the $ZnAl_2O_4$:0.01 %Cr^{3+} phosphor can be tuned slightly be varying the AT.

References

[1] F.M. Stringhini, E.L. Folleto, D. Sallet, D.A. Berthol, O. Chiavonefilho, and C.A.O. Nascimento, *J. Alloy Compd.* 558, 305 (2014).

[2] E.M.A. Jamal, D.S. Kumar, and M.R. Anantharaman, *Bull Mater Sci.* 34, 251 (2011).

[3] W.S. Tzing, and W.H. Taun, *J. Mater Sci. Lett.* 15, 1395 (1996).

[4] A.R. Phani, M. Passacantando, and S. Aantucci, *Mater. Chem. Phys.* 68, 66 (2001).

[5] S. Battiston, C. Rigo, E. da Cruz Severo, M.A. Mazutti, R.C. Kuhn, A. Gündel, and E.L. Foletto, *Mater. Res.* 17 (3), 734 (2014).

[6] S.V. Motloung, F.B. Dejene, H.C. Swart, and O.M. Ntwaeaborwa, *J. Sol-Gel Sci. Technol.* 70, 422 (2014).

[7] S.V. Motloung, M. Tsega, F.B. Dejene, H.C. Swart, O.M. Ntwaeaborwa, L.F. Koao, T.E. Motaung, and M.J. Hato, *J. Alloy Compd.* 677, 72 (2016).

[8] S.V. Motloung, F.B. Dejene, H.C. Swart, and O.M. Ntwaeaborwa, *Ceram. Int.* 5, 6776 (2015).

[9] M. Kumar, M. Mohopatra, and V. Natarajan, *J. Lumin.* 149, 118 (2014).

[10] A. Fernandez-Osorio, C. E. Riveria, and J. Charez, *Proceedings of the World Congress on New Technologies*. Paper No 360 (2015).

[11] M.G. Brik, J. Papan, D.J. Jovanovic, M.D. Dramicanin, *J. Lumin.* 177, 145 (2016).

[12] G. Rani, *Powder Technol.* 312, 354 (2017).

[13] S.K. Sampath, D.G. Kanhere, and R. Pandey, *J. Phys. Condens. Matter* 11, 3635 (1999).

[14] J. Wrzyszcz, M. Zawadzki, J. Trawczynski, H. Grabowska, and W. Mista, *Appl. Catal. A Gen.* 210, 263 (2001).

[15] J.J. Kingsley, K. Suresh, and K.C. Patil, *J. Mater. Sci.* 25, 1305 (1990).

[16] Y.H. Lin, Z.T. Zhang, F. Zhang, Z.L. Tang, and Q.M. Chen, *Mater. Chem. Phys.* 65, 103 (2000).

[17] T.Y. Peng, H.J. Liu, H.P. Yang, and C.H. Yan, *Mater. Chem. Phys.* 85, 68 (2004).

[118] D. Ravichandran, S.T. Johnson, S. Erdei, R. Roy, and W.B. White, Displays 19, 197 (1999).

[19] A.A. Da Silva, A. de Souza Goncalves, and M.R. Davolos, *J. Sol-Gel Sci. Technol.* 49, 101 (2009).

[20] B.D. Cullity, *1956 Elements of X-ray Diffraction*, 2nd ed. (Addison Wesley, 1978), pp. 285–286.
[21] S. V. Motloung, F. B. Dejene, O.M. Ntwaeaborwa, and H.C. Swart, Mater. Res. Express 1, 045029 (2014).

[22] S-F. Wang, G-Z. Sun, L-M. Fang, L. Lei, X. Xiang, and X-T. Zu, *Sci. Rep.* 5, 12849 (2015).

[23] Z. Xia, J. Zhuang, H. Liu, and L. Liao, *J. Phys. D: Appl. Phys.* 45 (7pp), 015302 (2012).

[24] ⟨http://www.mathworks.com/matlabcentral/fileexchange/29620-cie-coordinate-calculator⟩ 2012 (accessed 21.10.12).